Journals Pub

International Journal of
Composite and Constituent Materials

ISSN: 2456-5237
Volume 10, Issue 2, 2024
DOI (Journal): 10.37628/IJCCM

https://chemical.journalspub.info/index.php?journal=JCSCR

Review IJCCM

Structural, Optical, and Antibacterial Properties of $NiCr_2O_4/NiO$ Nanocomposite Synthesized by a Facile Microplasma Electrochemical Process

Afaq Khaliq[1,*], Muhammad Nabeel Sharif[2]

Abstract

Nowadays increasing severity of environmental pollution and antibiotic resistance poses significant global challenges, particularly due to the accumulation of organic pollutants from industrialization and the proliferation of antibiotic-resistant bacteria, which jeopardize ecosystems and public health. To address these issues, the development of advanced nanocomposites with photocatalytic and antimicrobial properties is of paramount importance. This article reports the synthesis of $NiCr_2O_4/NiO$ nanocomposite conducted in the current study via atmospheric pressure microplasma (AMP) electrochemical method. The synthesized nanocomposite's optical, structural, morphological, and compositional characteristics were thoroughly examined using UV-visible spectroscopy, X-ray diffraction (XRD), scanning electron microscopy (SEM), and Fourier-transform infrared (FTIR) spectroscopy. XRD analysis confirmed the crystalline structure of the nanocomposite, indicating the presence of a cubic spinel phase of $NiCr_2O_4$ (space group Fd-3m) and a cubic phase of NiO, with a crystallite size of 24.2 nm. SEM analysis demonstrated that nanocomposite exhibited a spherical-like morphology. FTIR spectra showed characteristic metal-oxygen ($Ni-O$ and $Cr-O$) stretching vibrations at $538\ cm^{-1}$ and $617\ cm^{-1}$. UV-visible absorption spectra revealed a broad absorption peak at 377 nm, and the nanomaterial's optical energy bandgap was estimated to be 2.4 eV. These findings highlight the potential of the $NiCr_2O_4/NiO$ nanocomposite for applications in environmental remediation and antimicrobial treatments.

Keywords: Nickel chromite, atmospheric pressure microplasma, spinel structure

INTRODUCTION

In recent decades, transition metal oxide has emerged as a significant area of scientific investigation, owing to their distinctive properties, such as adaptable characteristics, and superior catalytic performance. These attributes, coupled with the ability to finely tune them through advanced synthesis techniques, have considerably expanded their potential applications. Transition metal oxides are now widely recognized for their role in fields including energy storage, such as electrical, photocatalytic, optical, and antimicrobial, which are extremely important due to their technological applications [1]. The heightened focus on these nanomaterials emphasizes their critical importance in advancing the frontiers of modern ingredients science and technology [2–4]. The applications of transition metal oxides, such as ZnO, TiO_2, CuO, ZrO_2, Fe_3O_4, MgO, chromium oxide (Cr_2O_3), nickel oxide (NiO),

***Author for Correspondence**
Afaq Khaliq
E-mail: afaqkhaliq2016@gmail.com

[1]Student, Nano-Scale Physics Laboratory, Department of Physics, Air University, Islamabad, Pakistan.
[2]Student, Department of Physics, University of Poonch Rawalakot, Rawalakot, Pakistan.

Received Date: October 10, 2024
Accepted Date: October 14, 2024
Published Date

Citation: Afaq Khaliq, Muhammad Nabeel Sharif. Structural, Optical, and Antibacterial Properties of $NiCr_2O_4/NiO$ Nanocomposite Synthesized by a Facile Microplasma Electrochemical Process. International Journal of Composite and Constituent Materials. 2024; 10(2): 1–12p.

and MnO_2, etc., such as including chemicals, optoelectronics, aerospace, consumer goods, energy storage, semiconductors, environmental solutions, coatings, optics, cosmetics, food packaging, energy, textiles, paints, next-generation, medicine, catalysis, sensing, and plastics are just a few of the industries [5–8].

The properties of binary metal oxides make them highly attractive for an extensive range of applications, predominantly due to their capability to interact with biological systems. This capability has become increasingly vital in current years, primarily due to the rising issue of bacterial resistance. Binary transition metal oxides exhibit significantly superior properties compared to their corresponding oxides of NiO and Cr_2O_3 [9–12]. Binary metal oxide plays an important role in their potential applications as electrode materials for electrochemical films, supercapacitors, lithium-ion batteries, photocatalytic materials, gas sensors, fuel cells, conversion technologies, and as efficient for power generation [13, 14]. The efficient synthesis of binary metal oxide with controlled shapes, sizes, compositions, appropriate bandgap, stability, nontoxicity, better structural stability, and electronic conductivity [1, 15]. Transition metal oxides, such as Cr_2O_3, ZnO, NiO, MnO_2, and Cu_2O and their well-controlled structural nanocomposites, such as $NiCo_2O_4$, $NiCo_2O_4$/NiO, Co_2O_4/NiO, $CuCr_2O_4$, $NiCr_2O_4$, $ZnCr_2O_4$, $NiCr_2O_4$/NiO, and $CuCo_2O_4$/CuO, etc. have attracted attention for various important technological applications as the degradation of organic dyes in photocatalytic materials, remove the pollutants from wastewater and including the biomedical applications [16–26]. This is owing to the significant properties of the chosen metal oxides, such as NiO and Cr_2O_3 nanoparticles, which have an extensive variety of applications [27]. One of the promising transition metal oxides is nickel oxide (NiO) with a crystalline structure and a bandgap of 3.6 eV to 4.0 eV. One of the significant p-type nickel oxide semiconductors that has attracted increasing industrial and technological interest. This interest has mainly to do with its properties of nickel oxide has been used in a variety of uses including catalysts, magnetic material, non-enzymatic glucose sensors, fuel cells, anticancer, solar cells, dye-sensitized photocathodes, and a diversity of electronic devices [20, 28–29]. An important transition metal chromium oxide has hexagonal close-packed (HCP) crystal structures and p-type semiconductor metal oxide with a bandgap of 3.0eV to 3.4eV [30–32]. It is technologically interesting with attractive because of its good catalytic, magnetic, decent optical, high thermal stability, electrical, gas sensing, and physicochemical properties [33, 34]. Cr_2O_3 is an antiferromagnetic material and has numerous performances, such as solar energy collectors, optoelectronics devices, heterogeneous catalysts, refractory materials, inks, paints, and a variety of industries [35–37]. Several types of chromium oxide have been reported, including CrO_2, CrO_3, Cr_2O_3, CrO_4, Cr_2O_5, and Cr_2O_3. This interesting transition metal oxide is very important because it is widely used in abundant industries and can be applied to many areas, such as pigments, catalysts, dye, corrosion-resistant materials, coating material, hydrogen storage materials, gas sensors, solar energy applications, biomedical tools, and electrode materials for lithium material, etc. [38, 39]. As a result of these appreciated applications, the range of Cr_2O_3 nanomaterials corresponds to significant properties.

Spinel's Spinel oxides represent an important class of binary metal oxides characterized by a cubic crystal structure, typically belonging to the space group of Fd3m. These materials are characterized by the chemical formula AB_2O_4, in which B denotes a trivalent cation and A denotes a divalent cation [40–42]. $NiCr_2O_4$, is a notable member of this family, functioning as both a ferrimagnetic material and a p-type semiconductor. $NiCr_2O_4$ belongs to the chromite family and features a typical spinel structure, with Ni^{+2} ions located at the tetrahedral (A) sitesand Cr^{+3} ions occupying the octahedral (B) sites [43–46]. Nickel chromite with a normal spinel-type structure has achieved excellent materials due to its excellent structural, electrical, thermal (high melting point at 2300°C), optical (narrow bandgap), excellent catalytic, magnetic, sensing, physical-chemical properties, etc. [47, 48]. The interesting spinel compounds of nickel chromite ($NiCr_2O_4$/NiO), with potential applications, include gas sensors, pigments, lithium-ion batteries, full cells, magnetic materials, thermal mechanical

devices, electronic apparatus, semiconductors, chemical industrial fields, etc. [49]. It is superior to know that the practical use of $NiCr_2O_4$ depends on its particle size, purity, and morphology.

The $NiCr_2O_4/NiO$ cubic spinel phase was selected for this study due to its outstanding properties, such as superior electronic conductivity, improved electrochemical performance, and significant electrochemical activity. Additionally, $NiCr_2O_4$ offers a low-cost, environmentally friendly, and naturally abundant option with high theoretical capacity, making it a promising candidate for electrode materials. Nickel chromite can be synthesized using numerous methods, such as spray drying, hydrothermal, thermal treatment, wet co-precipitation, sol-gel, sol-spray, ball milling, co-precipitation, solid-state reactions, combustion, and thermal decomposition processes [50–54]. By carefully selecting and controlling the starting materials and synthesis conditions, these techniques enable the efficient production of the nanocomposite with optimal yield.These methods were used to synthesize the $NiCr_2O_4/NiO$, but the resulting nanocomposite did not have uniform size or good chemical and physical properties. The technique has attracted the attention of various other methods and advantages of a microplasma [55], this technique in comparison to other synthesis routes, avoids the production of nanocomposite's containment issues. This method is the most ideal for the production of materials since it is a very simple, faster, worldwide friendly method with a low cost of production, simple procedure use, nontoxic, high electrochemical properties, nontoxic elements are used in this method, and time-consuming procedure when compared to other synthetic techniques. Atmospheric microplasma has a wide range of applications, including high-pressure fluorescent lamps, plasma flashlights, activation flashes, radiation sources, microchemical analysis systems, gas analyzers, and environmental technologies [56–57]. This study successfully produced a $NiCr_2O_4/NiO$ nanocomposite (NC) using an electrochemical method, with nickel and chromium nitrates as the sole precursors. The characteristics of the developed nanocomposite were investigated utilizing a variety of spectroscopic and microscopic techniques. The objective of this assessment is to develop the synthesis of $NiCr_2O_4/NiO$ NC for use in antibacterial applications.$NiCr_2O_4/NiO$ NC also reveals antimicrobial activity against a gram-negative pathogen and gram-positive pathogen [58]. To the highest standard of our knowledge, synthesized NC utilizing the electrochemical technique, characterized by different techniques and antibacterial properties of nanocomposite has not yet been described.

EXPERIMENTAL PROCEDURE

Materials

The $NiCr_2O_4/NiO$ nanocomposite was synthesized using the precursors $Cr(NO_3)_3{\bullet}9H_2O$ and $Ni(NO_3)_2{\bullet}6H_2O$ without the need for further purification.

Synthesis of $NiCr_2O_4/NiO$ nanocomposite

Figure 1 illustrates that the experimental setup used facile electrochemical synthesis. The $NiCr_2O_4/NiO$ nanocomposite was prepared using a custom-developed microplasma electrochemical technique. In this process, the stainless steel anode was immersed in the electrolyte solution, while argon gas was delivered to the cathode through a stainless steel capillary tube, with a 2 cm gap between the electrodes. The anode, measuring length in 2 cm and width in 1 cm, was employed in themicroplasma setup. $Ni(NO_3)_2{\bullet}6H_2O$ and $Cr(NO_3)_3{\bullet}9H_2O$ were dissolved in deionized water in a 1:1 molar ratio to form the electrolyte solution, leading to the dissociation of Ni^{+2} ions and Cr^{+3} ions. A DC power supply (IT6726V, 1200V/5A) was connected to the setup, with a ballast resistor (R = 50 kΩ) maintaining stability. To initiate the discharge at the surface of the electrolyte solution, a high voltage of 1.2 kV and a discharge current of 0.01 A were applied simultaneously. Electrons from the argon plasma interacted with the water molecules, inducing redox reactions in which hydroxide ions (OH^-) reacted with ions to form the bimetallic hydroxide complex [$NiCr_2(OH)_6$], where hydroxide ions (OH^-) reacted with Ni^{+2} and Cr^{+3} ions to form a bimetallic hydroxide complex, which subsequently transformed into the $NiCr_2O_4/NiO$ nanocomposite. Within the first 10 minutes of the reaction, a green color appeared at the surface of the solution, indicating the fabrication of the nickel-chromium oxide nanocomposite. As the reaction progressed, the nanoparticles dispersed throughout the solution,

turning it a dark green color. The reaction was completed after 40 minutes, and the solution was permitted to cool to room temperature. After collecting the precipitate, it was double-washed with ethanol and deionized water before being dehydrated for 24 hours at 110°C in an electric oven. The material was calcined at 600°C for 4 hours to remove any remaining byproducts [59].

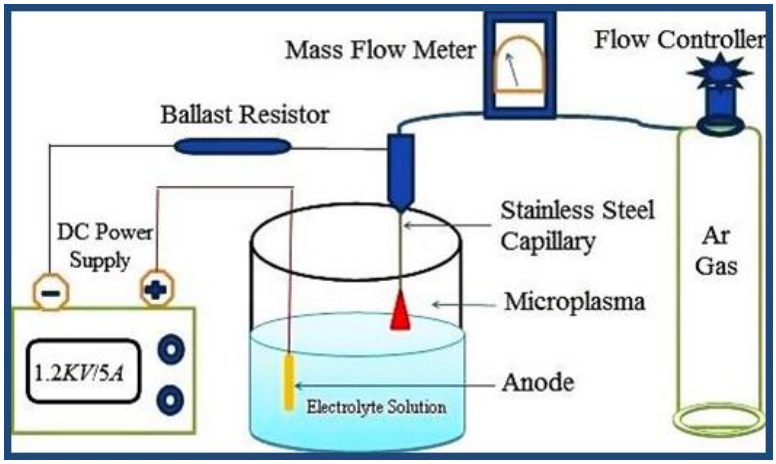

Figure 1. The synthesis geometry of atmospheric pressure microplasma (AMP) for $NiCr_2O_4$/NiO NC.

Characterization Technique

Various advanced techniques were employed to characterize the $NiCr_2O_4$/NiO nanocomposite during its formation. X-ray diffraction (XRD) analysis was employed to investigate the structural characteristics of the $NiCr_2O_4$/NiO nanomaterial, focusing on the identification of crystallite size, the cubic spinel phase, and other structural properties of the synthesized nanocomposite. The XRD measurements were conducted using a diffractometer and an X'Pert PRO 3040/60. Scanning electron microscopy (SEM) was conducted using a Jeol JSM-6510LV to examine the morphology of the nanocomposite. Fourier transform infrared (FTIR) spectroscopy was performed with a Perkin Elmer model 1650, acquiring IR spectra in the $400-4000\ cm^{-1}$ range to elucidate the vibration modes and functional groups. The bandgap of the $NiCr_2O_4$/NiO nanocomposite was determined, and the optical absorbance spectra were analyzed using UV-visible spectroscopy (PerkinElmer Lambda 950), evaluating absorbances in both the visible ($400-800$ nm) and UV ($200-400$ nm) regions.

Antibacterial Activity

The antimicrobial activity of the synthesized $NiCr_2O_4$/NiO nanocomposite was assessed using the disc diffusion method. The test organisms were prepared by cultivating a bacterial suspension in a nutrient broth medium (CM1 oxide). A large volume of bacterial culture was inoculated into 25 mL of nutrient broth and incubated on a rotary shaker at 37°C for 24 hours. Next, the recently prepared Muller Hinton agar medium (CMO 337 oxide) was mixed with the overnight culture and poured into sterilized Petri dishes, maintaining the medium at 45°C. The plates were allowed to solidify at room temperature under a laminar stream. Each solidified agar plate was drilled with six wells, each 5 mm in diameter. Approximately 30 µL of a solution containing 1 mg of $NiCr_2O_4$/NiO nanocomposite powder dissolved. A sample was treated with dimethyl sulfoxide (DMSO, Sigma-Aldrich, 99.5% concentration). The antibacterial activity was determined by measuring the zones of inhibition following an incubation period of 24 hours at 37°C. The inhibition zone diameters were recorded, and the standard error was calculated to ensure accuracy [3, 19].

RESULTS AND DISCUSSION

Structural Analysis

Figure 2 represents the XRD structure of $NiCr_2O_4$/NiO NC prepared with the 1:1 ratio of $Cr(NO_3)_3 \cdot 9H_2O$ and $Ni(NO_3)_2 \cdot 6H_2O$. Upon calcination at 600°C for 4 hours, the phases of

$NiCr_2O_4$ and NiO were successfully synthesized. XRD was employed to explore the crystal constructions and identify the phases of the produced nanocomposite. The observed diffraction peaks at 2θ values of $18.08°, 30.28°, 35.75°, 54.87°$, and $57.7°$ correspond to Miller indices assigned to the (111), (220), (311), (422), and (511) planes of the face-centered cubic spinel $NiCr^2O^4$ phase, which has a space group of Fd-3m (space group number 227, JCPDS Card No. 00-023-1271). The diffraction peaks at $43.2°$ and $63.2°$ can be assigned. To the (400) and (440) crystal planes of the cubic phase NiO, which has a space group of Fm3m (JCPDS Card No. 00-047-1049). The structure of peaks resembles the FCC cubic phase of the $NiCr_2O_4$, with calculated the lattice parameters of $a = b = c = 8.3160$ Å and a volume of 575.10 Å^3. The most intense peak, centered at $2\theta = 35.75°$, corresponds to the (311) crystal plane, indicating good crystallinity and confirming the presence of $NiCr_2O_4$. The crystallite size of synthesized $NiCr_2O_4$/NiO nanocomposite was approximately 24.2 nm, as using the Debye-Scherrer formula determined d-spacing and lattice parameters [60].

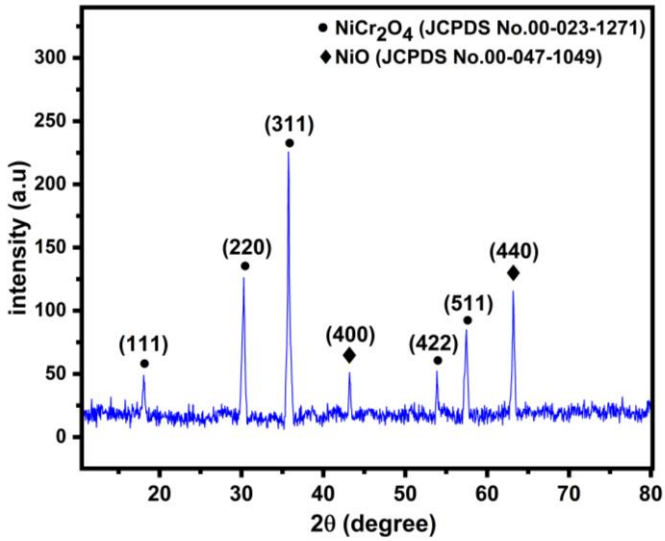

Figure 2. Structural patterns of prepared $NiCr_2O_4$/NiO nanocomposite.

Morphological Analysis of $NiCr_2O_4$/NiO NC

Scanning Electron Microscopy (SEM) was employed to analyze the shapes, sizes, and surface morphologies of the obtained sample nickel chromite ($NiCr_2O_4$/NiO) NC, which illustrates the surface morphology of nanocomposite. Figure 3 shows that the SEM images of $NiCr_2O_4$/NiO NC were obtained by SEM with two different magnifications in the nanometer and micrometer range. SEM images show that the sample as-grown has a well-distributed spherical-like morphology. Highly agglomerated images of $NiCr_2O_4$/NiO NC calcined at 600°C were obtained. $NiCr_2O_4$/NiO NC images show well-uniform agglomerated morphologies with a well-dispersed structure. SEM images revealed that the average particle size of the nanocomposite ranged from 33 to 61.6 nm. The morphology of the nanocomposite was significantly influenced by its inherent crystal structure and the processing conditions utilized during synthesis [61].

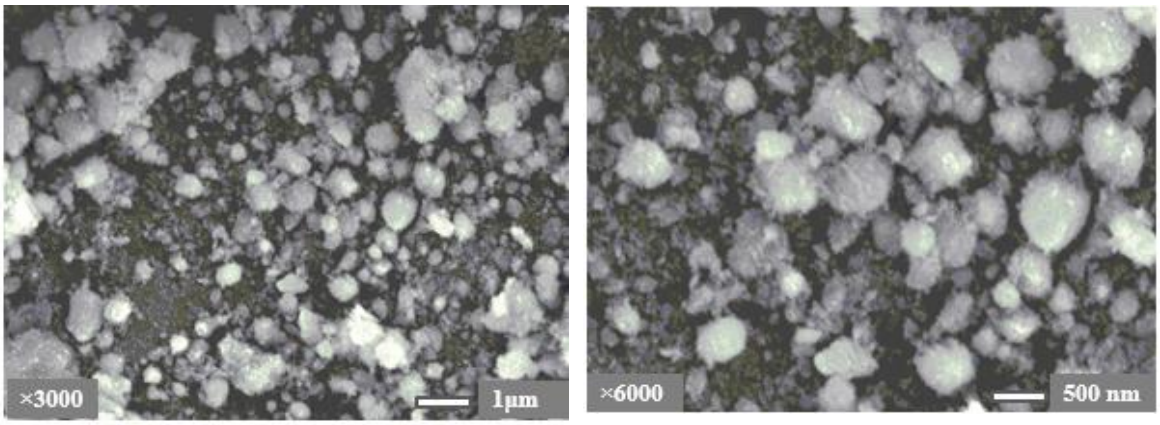

Figure 3. $NiCr_2O_4$/NiO NC SEM images at different magnifications and calcined at 600° for 4 hours.

FTIR Analysis of $NiCr_2O_4$/NiO NC

Figure 4 shows that the FTIR spectra of the prepared $NiCr_2O_4$/NiO NC performed in the wavenumber range of $400-4000\ cm^{-1}$. This spectroscopy was employed to analyze the functional groups and vibrational stretching modes present in the synthesized $NiCr_2O_4$/NiO sample. The peak at $3407\ cm^{-1}$ is attributed to $O-H$ vibrational stretching, while the bending vibrational modes of interlayer water molecules correspond to the peak at $1649\ cm^{-1}$. Two distinct bands at $538\ cm^{-1}$ and $617\ cm^{-1}$, associated with the Fd-3m space group (No. 227), indicate the stretching vibrations related to metal-oxygen bonds ($Ni-O$ and $Cr-O$) in the cubic spinel phase of the $NiCr_2O_4$/NiO nanostructures. Furthermore, the peak at $2026\ cm^{-1}$ is attributed to the C–C stretching vibrations. Various peaks corresponding to dissimilar bond stretching vibrations were observed. The stretching and bending vibrations of $O-H, C-C, C=C, C-N, C-H, Cr-O$, and $Ni-O$ were recorded at wave numbers of $3407\ cm^{-1}, 2026\ cm^{-1}, 1649\ cm^{-1}, 1021\ cm^{-1}, 882\ cm^{-1}, 617\ cm^{-1}$, and $538\ cm^{-1}$, respectively. The dispersal of Ni^{+2} ions in the octahedral sites and Cr^{+3} ions in the tetrahedral sites of the AB_2O_4 lattice contributes to the observed bands in the spinel structure [62, 63]. The interpretation of the infrared absorption spectrum provides insights into the chemical bonds within the molecule.

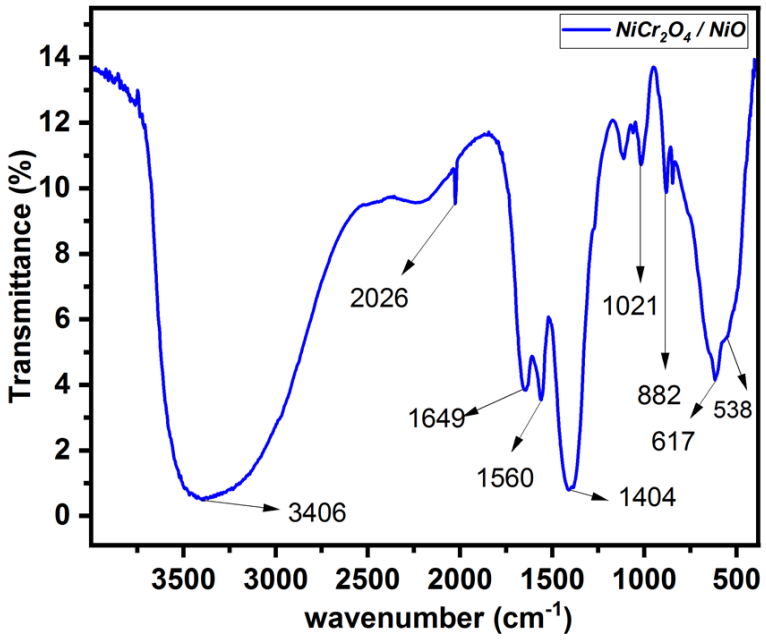

Figure 4. FTIR spectra of prepared $NiCr_2O_4$ nanocomposite.

UV-visible Analysis of $NiCr_2O_4/NiO$ NC

Figure 5(a) shows the UV-visible absorption ensembles of $NiCr_2O_4/NiO$ *NC* and represents the plot of absorbance versus wavelength of the prepared sample. In spectra, we have seen that the maximum absorption peaks lie at the 377 nm range. The UV-visible spectrum of the sample was acquired over a wavelength range of 200–800 nm.

Tauc's relation, which provides a connection between the absorbance coefficient (α) and photon energy(hυ), was used to calculate the bandgap of the synthesized nanocomposite.

$$(\alpha h\upsilon) = C(h\upsilon - Eg)^n$$

In this equation, hυ represents the energy of the incident photon, C is a proportionality constant, Eg is the bandgap energy, and n denotes the type of electronic transition. Specifically, while n = 1/2 is applicable for endorsed direct transitions, n = 2 corresponds to indirect band transitions. Figure 5b illustrates the plots of $(\alpha h\upsilon)^2$ versus hυ, with n set to 1/2 for the acceptable direct transitions in the $NiCr_2O_4/NiO$. The optical absorption spectrum of the as-prepared NC was obtained, and Tauc's equation was applied to calculate the energy bandgap, Eg, yielding a value of 2.4 eV. The bandgap energy (Eg) was determined by extrapolating the linear region of the plotted graphs along the hυ-axis. The calculated bandgap energy of the NC exceeds previously reported values [64].

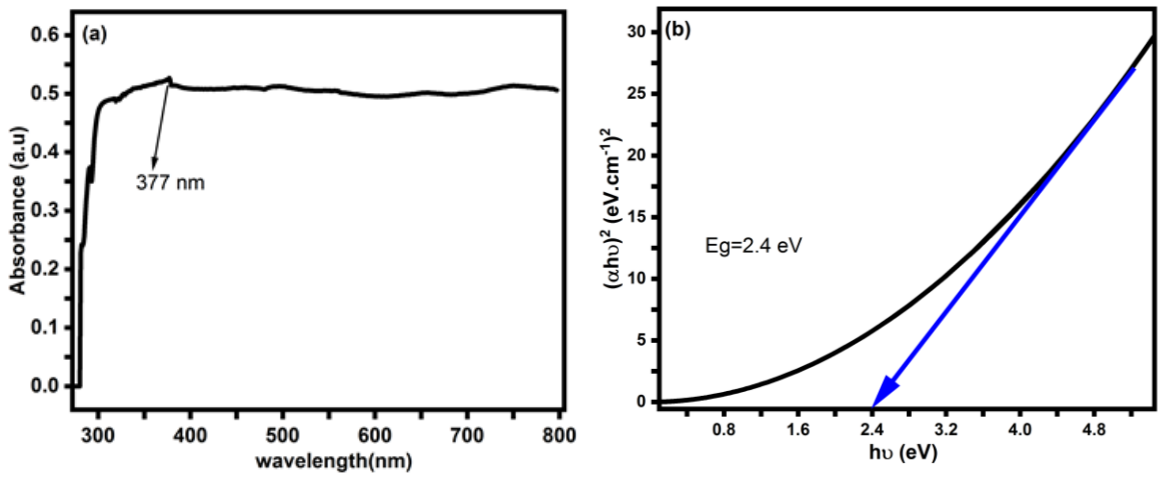

Figure 5. (a) UV-Visible absorption spectra of prepared $NiCr_2O_4/NiO$ NC sample, and (b) plots of $(\alpha h\upsilon)^2$ versus Energy(hυ).

Antibacterial Activity

The antibacterial properties of the synthesized $NiCr_2O_4/NiO$ nanocomposite were evaluated utilizing the disc diffusion test. The results show that the concentrations of the nanocomposite demonstrate a higher zone of inhibition. The measured values of different inhibition zones are 29 mm to 40 mm for *Staphylococcus aureus* and 16 mm to 37 mm for *Escherichia coli*. The antimicrobial activity mechanism of nickel chromite ($NiCr_2O_4$) NCs is not completely known [65]. According to a literature review, chromium oxide (Cr_2O_3) plays an energetic role in antibacterial activity. The electrostatic interaction between the positive chromium ion and the negative cell membrane of bacteria causes the inactivation of DNA and protein. In another article, author investigated that the antimicrobial process of Cr_2O_3 NPs shows more activity which depends upon the nanoparticle's concentrations [66]. The nanoparticle's growth on the cell membrane of the microorganisms *S. aureus* and *E. coli* causes permeability, which leads the cell death. The bactericidal phenomenon of positively charged chromium and negative nickel nanomaterial is very problematic to explain, therefore we expect some other conceivable mechanisms [59]. The development of the asymmetrically shaped pits

in the outside membrane and variation in membrane permeability by Cr_2O_3 NPs was investigated. This phenomenon is attributed to the abrupt release of membrane proteins and lipopolysaccharide molecules. Similar mechanisms have been explored in previous studies, which reported that Cr_2O_3 nanoparticles reasonharm to the cell membrane of *E. coli*. The exact mechanism of protein and cell membrane damage by Cr_2O_3 NPs was still a big challenge [67]. These free radicals attack the bacterial cell wall and damage it. They investigated the effect of free radical generation under the treatment of Cr_2O_3 NPs on damaging the cell wall of gram-negative bacterial membranes. Interestingly, the NiONPs inhibit both bacterial strains, but they are most effective against gram-negative bacteria. Earlier studies have also shown that NiONPs have better antiseptic activity against gram-negative bacteria and gram-positive bacteria Table 1. We used prepared NC to evaluate their antibacterial activity in contradiction of both bacteria (Figure 6) [65, 67].

Table 1. Against *E. coli* and *S. aureus* antimicrobial activity of $NiCr_2O_4$/NiO.

Pathogens	**NC in mg/ml**			**Zones of Inhibitions (mm)**		
E.coli	35	45	55	16.0 ± 0.04	35.0 ± 0.01	37.0 ± 0.06
S. aureus	35	45	55	29.00 ± 0.05	38.01 ± 0.01	40.0 ± 0.02

gt

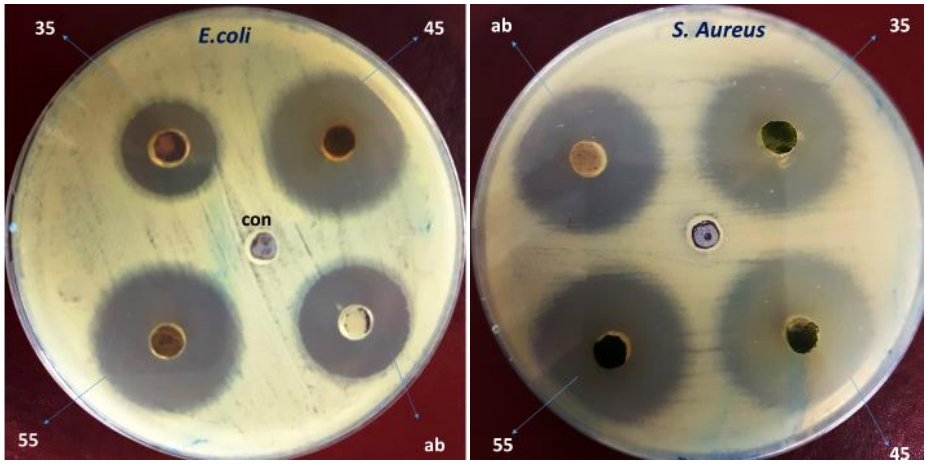

Figure 6. Antibacterial activity of $NiCr_2O_4$/NiO nanocomposite.

CONCLUSION

In this study, $NiCr_2O_4$/NiO nanocomposite was successfully synthesized using the electrochemical method, employing nickel and chromium nitrates as precursors. The properties of the produced nanocomposite were thoroughly analyzed through various characterization techniques. Upon calcination at 600°C, the formation of $NiCr_2O_4$/NiO and NiO phases was confirmed, indicating that this temperature is optimal for obtaining normal cubic spinel structures of nickel chromite. XRD analysis, performed using the X'Pert PRO 3040/60, validated the existence of the cubic phase and normal spinel phase of NiO and $NiCr_2O_4$. The crystallite size of the $NiCr_2O_4$/NiO nanocomposite was found to be 24.2 nm, calculated using Debye-Scherrer's formula. Analysis through SEM indicated that the synthesized $NiCr_2O_4$/NiO nanocomposite had a spherical morphology. FTIR spectroscopy further supported these findings, with significant stretching vibrations in the $NiCr_2O_4$ spinel nanostructures observed at 538 cm^{-1} and 617 cm^{-1}, corresponding to the Fd-3m space group. The bandgap energy of the $NiCr_2O_4$/NiO nanocomposite was determined to be 2.4 eV. Antibacterial activity studies demonstrated that the assisted microplasma-synthesized nanocomposite exhibited significant antibacterial properties against both bacteria.

REFERENCES

1. Arulraj J, Mathew M. Photocatalytic applications of transition metal and metal oxide nanoparticles. International Journal of Advanced Scientific Research and Management. 2019;4(4):389–401.
2. Agnihotri AS, Varghese A, Nidhin M. Transition metal oxides in electrochemical and bio sensing: A state-of-art review. Appl Surf Sci Adv. 2021;4:100072. doi: 10.1016/j.apsadv.2021.100072.
3. Iqbal T, Mukhtar M, Khan MA, Khan R. Atmospheric pressure microplasma assisted growth of silver nanosheets and their inhibitory action against bacteria of clinical interest. Mater Res Express. 2016;3(12):125019. doi: 10.1088/2053-1591/3/12/125019.
4. Iqbal T, Aziz A, Khan MA, Andleeb S. Surfactant assisted synthesis of ZnO nanostructures using atmospheric pressure microplasma electrochemical process with antibacterial applications. MSEB. 2018;228:153–159. doi: 10.1016/j.mseb.2017.11.027.
5. Ahuja P, Ujjain SK, Kanojia R, Attri P. Transition metal oxides and their composites for photocatalytic dye degradation. J Compos Sci. 2021;5(3):82. doi: 10.3390/jcs5030082.
6. Danish MSS, Estrella LL, Alemaida IMA, Lisin A, Moiseev N, Ahmadi M, et al. Photocatalytic applications of metal oxides for sustainable environmental remediation. Metals, 2021;11(1):80. doi: 10.3390/met11010080.
7. Shafique M, Iqbal T, Khan MA, Naeem M, Ahmed I, Ahmad P, et al. Structural, optical, electrical, and photocatalytic properties of nickel cobaltite ($NiCo_2O_4$) nanocomposite fabricated by a facile microplasma electrochemical process. J Electron Mater. 2021;50:629–639. doi: 10.1007/s11664-020-08573-1.
8. Haider AJ, Al-Anbari R, Sami HM, Haider MJ. Photocatalytic activity of nickel oxide. JMR&T. 2019;8(3):2802–2808. doi: 10.1016/j.jmrt.2019.02.018.
9. Lei Z, Lee JM, Singh G, Sathish CI, Chu X, Al-Muhtaseb AH, et al. Recent advances of layered-transition metal oxides for energy-related applications. Energy Storage Mater. 2021;36:514–550. doi: 10.1016/j.ensm.2021.01.004.
10. Mei J, Liao T, Ayoko GA, Sun Z. Two-dimensional bismuth oxide heterostructured nanosheets for lithium-and sodium-ion storages. ACS Appl Mater Interfaces. 2019;11(31):28205–28212. doi: 10.1021/acsami.9b09882.
11. Yarbrough R, Davis K, Dawood S, Rathnayake H. A sol–gel synthesis to prepare size and shape-controlled mesoporous nanostructures of binary (II–VI) metal oxides. RSC Adv. 2020;10(24):14134–14146.
12. Sanchez JS, Pendashteh A, Palma J, Anderson M, Marcilla R. Porous NiCoMn ternary metal oxide/graphene nanocomposites for high performance hybrid energy storage devices. Electrochim Acta. 2018;279:44–56. doi: 10.1016/j.electacta.2018.05.072.
13. Iyer MS, Rajangam I. Hybrid nanostructures made of porous binary transition metal oxides for high performance asymmetric supercapacitor application. Journal of Energy Storage, 2023;67(1):107530. doi: 10.1016/j.est.2023.107530.
14. Liguang W, Changming Z, Zhaoming T, Songliu Y. Exchange bias and training effect in $NiCr_2O_4/Cr_2O_3$ composite. JMR&T. 2015;30(21):3252–3258. doi: 10.1557/jmr.2015.272.
15. Ma J, Ni S, Zhang J, Yang X, Zhang L. The electrochemical performance of nickel chromium oxide as a new anode material for lithium ion batteries. Electrochim Acta. 2015;176:1420–1426. doi: 10.1016/j.electacta.2015.07.071.
16. Javed M, Khan AA, Kazmi J, Mohamed MA, Khan MN, Hussain M, et al. Dielectric relaxation and small polaron hopping transport in sol-gel-derived $NiCr_2O_4$ spinel chromite. Mater Res Bull. 2021;138:111242. doi: 10.1016/j.materresbull.2021.111242.
17. Gao H, Guo J, Li Y, Xie C, Li X, Liu L, et al. Highly selective and sensitive xylene gas sensor fabricated from $NiO/NiCr_2O_4$ p-p nanoparticles. Sens Actuators B Chem. 2019;284:305–315. doi: 10.1016/j.snb.2018.12.152.
18. Tomar A, Singh J, Singh SP, Rai AK. Designed synthesis of $CuCo_2O_4$/CuO nano-composite as a potential anode material for lithium ion batteries. Physica E Low Dimens Syst Nanostruct. 2020;116:113736.

19. Shafique M, Iqbal T, Mahmood H, Khan MA. Surfactant-assisted synthesis of $NiCo_2O_4$/NiO nanocomposite by facile atmospheric pressure microplasma electrochemical process with photocatalytic applications. J Mater Sci: Mater Electron. 2021;32(7):17865–17875. doi: 10.1007/s10854-021-06322-6
20. Shobeiri SA, Mousavi-Kamazani M, Beshkar F. Facile mechanical milling synthesis of $NiCr_2O_4$ using novel organometallic precursors and investigation of its photocatalytic activity. J Mater Sci: Mater Electron. 2017;28:8108–8115. doi: 10.1007/s10854-017-6517-2.
21. Mojallal S, Mohammadzadeh H, Aghaeinejad-Meybodi A, Jafari R. Effect of NiO–$NiCr_2O_4$ nano-oxides on the microstructural, mechanical and corrosion properties of Ni-coated carbon steel. Int J Min Met Mater. 2023;30(6):1078–1092. doi: 10.1007/s12613-022-2584-3.
22. Xu Y, Tian X, Fan Y, Sun Y. A formaldehyde gas sensor with improved gas response and sub-ppm level detection limit based on NiO/$NiFe_2O_4$ composite nanotetrahedrons. Sens Actuators B Chem. 2020;309:127719. doi: 10.1016/j.snb.2020.127719.
23. Tuyen TN, Quyen NDV, Lam TB. Synthesis of $Fe_xZn_{1-x}Cr_2O_4$ brown ceramic pigment by starch-assisted sol-gel process. HUJOS: Nat Sci. 2019;128(1B):13–19. doi: 10.26459/hueuni-jns.v128i1B.5245.
24. Mobini S, Meshkani F, Rezaei M. Surfactant-assisted hydrothermal synthesis of $CuCr_2O_4$ spinel catalyst and its application in CO oxidation process. J Environ Chem Eng. 2017;5(5):4906–4916. doi: 10.1016/j.jece.2017.09.027.
25. Mimouni R, Askri B, Larbi T, Amlouk M, Meftah A. Photocatalytic degradation and photo-generated hydrophilicity of methylene blue over ZnO/ZnCr2O4 nanocomposite under stimulated UV light irradiation. Inorg Chem Commun. 2020;115:107889. doi: 10.1016/j.inoche.2020.107889.
26. Namini AS, Delbari SA, Mousavi M, Ghasemi JB. Synthesis and characterization of novel ZnO/$NiCr_2O_4$ nanocomposite for water purification by degradation of tetracycline and phenol under visible light irradiation. Mater Res Bull. 2021;139:111247. doi: 10.1016/j.materresbull.2021.111247.
27. Liu Y, Huang M, Zhao J, Lu M, Zhou X, Lin Q, et al. One-pot synthesis of NiO/$NiCr_2O_4$ nanostructure as an efficient catalyst for urea electro-oxidation in alkaline media. J Electrochem Soc. 2020;167(6):066520. doi: 10.1149/1945-7111/ab8647.
28. Benrighi Y, Nasrallah N, Chaabane T, Sivasankar V, Darchen A, Baaloudj O. Photocatalytic performances of $ZnCr_2O_4$ nanoparticles for cephalosporins removal: Structural, optical and electrochemical properties. Opt Mater. 2021;115:111035. doi: 10.1016/j.optmat.2021.111035.
29. Mohammed GH, Hassan TB, Abdulhamied ZT. Structural characterization of NiO/Cr_2O_3 composites and hydrothermal synthesis, properties gas sensing. ANJS. 2018;21(1):59–64. doi: 10.22401/JNUS.21.1.10.
30. Jeba SV, Sebastiammal S, Sonia S, Fathima AL. Synthesis, growth mechanism and photocatalytic properties of nickel oxide (NiO) nanoflower: A hydrothermal process. Inorg Nano-Met Chem. 2020;51(10):1431–1441. doi: 10.1080/24701556.2020.1837163.
31. Al-Hada NM, Al-Ghaili AM, Kasim H, Saleh MA, Baqiah H, Liu J, et al. Nanofabrication of $(Cr_2O3)_x$ $(NiO)_{1-x}$ and the impact of precursor concentrations on nanoparticles conduct. JMR&T. 2021;11:252–263. doi: 10.1016/j.jmrt.2021.01.007.
32. Al-Hada NM, Kamari HM, Saleh MA, Flaifel MH, Al-Ghaili AM, Kasim H, et al. Morphological, structural and optical behaviour of PVA capped binary $(NiO)_{0.5}$ $(Cr_2O_3)_{0.5}$ nanoparticles produced via single step based thermal technique. Results Phys. 2020;17:103059. doi: 10.1016/j.rinp.2020.103059.
33. Govindharaj S, Nizar AM, Akilaa O, Shanmugam R, Thangavelu L. Green synthesis of tannic acid-mediated chromium oxide nanocomposites using acalypha indica and carica papaya leaf and its biomedical applications. Nanotechnol Percept. 2024;20(S7):304–326. doi: 10.62441/nano-ntp.v20iS7.25.
34. Anand GT, Nithiyavathi R, Ramesh R, Sundaram SJ, Kaviyarasu K. Structural and optical properties of nickel oxide nanoparticles: Investigation of antimicrobial applications. Surfaces and

Interfaces. 2020;18(8):100460. doi: 10.1016/j.surfin.2020.100460.
35. Bhardwaj P, Singh J, Kumar R, Kumar R, Verma V. Structural, optical and magnetic characterization of Ni^{2+} ions doped chromium oxide (Cr_2O_3) nanoparticles. Solid State Sci. 2021;115:106581. doi: 10.1016/j.solidstatesciences.2021.106581.
36. Khalaji D. Structural, Optical and magnetic studies of Cr_2O_3 nanoparticles prepared by microwave-assisted. Nanochem Res. 2021;6(1):18–24. doi: 10.1016/j.solidstatesciences.2021.106581.
37. Huang X, Fossati PC, Martinelli L, Bosonnet S, Latu-Romain L, Wouters Y. A DFT study of defects in paramagnetic Cr_2O_3. Phys Chem Chem Phys. 2022;24(17):10488–10498. doi: 10.1039/d1cp05756a.
38. Patil SP, Chaudhari RY, Nemade MS. Azadirachta indica leaves mediated green synthesis of metal oxide nanoparticles: A review. Talanta Open. 2022;5:100083. doi: 10.1016/j.talo.2022.100083.
39. Singh J, Kumar R, Verma V, Kumar R. Structural and optoelectronic properties of epitaxial Ni-substituted Cr_2O_3 thin films for p-type TCO applications. Mater Sci Semicond Process. 2021;123(12pp):105483. doi: 10.1016/j.mssp.2020.105483.
40. Nikolova MP, Chavali MS. Metal oxide nanoparticles as biomedical materials. Biomimetics. 2020;5(2):27. doi: 10.3390/biomimetics5020027.
41. Kirankumar V, Sumathi S. A review on photodegradation of organic pollutants using spinel oxide. Mater Today Chem. 2020;18:100355. doi: 10.1016/j.mtchem.2020.100355.
42. Pei Z, Zheng X, Li Z. Progress on synthesis and applications of Cr_2O_3 nanoparticles. J Nanosci Nanotechnol. 2016;16(5):4655–4671. doi: 10.1166/jnn.2016.12602.
43. Permatasari TW, Wijaya HW, Taufiq A, Dasna IW. The effect of addition Ni^{+2} to Cr_2O_3 and its potential characterization as anode potassium ion battery. J Phys Conf Ser. 2021;1811(1):012032. doi: 10.1088/1742-6596/1811/1/012032.
44. Bakar SA, Soltani N, Yunus WMM, Saion E, Bahrami A. Structural and paramagnetic behavior of spinel $NiCr_2O_4$ nanoparticles synthesized by thermal treatment method: Effect of calcination temperature. Solid State Commun. 2014;192:15–19. doi: 10.1016/j.ssc.2014.05.002.
45. Vasil'kov O, Barinova O, Kirsanova S, Marnautov N, Elfimov A. Ceramic black pigments based on chromium-nickel spinel $NiCr_2O_4$. GC. 2017;74(8):236–239. doi: 10.1007/s10717-017-9970-8.
46. Wang D, Mi Q, Zhang H, Li G, Zhang D. Sensitive xylene gas sensor based on NiO-$NiCo_2O_4$ hierarchical spherical structure constructed with nanorods. IEEE Sensors J. 2022;22(11):10346–10352.
47. Mondal PP, Mahapatra PL, Das S, Saha D. Study on the novel capacitive moisture sensing behaviour of nickel chromite nanoparticle based thick film. Measurement, 2020;163(5):107992. doi: 10.1016/j.measurement.2020.107992.
48. Ragupathi C, Narayanan S, Tamizhdurai P, Govindasamy M, ALOthman ZA, Al-Anazy MM. Tuning magnetic, electronic, and optical properties of Mn-doped $NiCr_2O_4$ via microwave method. J Saudi Chem Soc. 2021;25(7):101275. doi: 10.1016/j.jscs.2021.101275.
49. Abbasi A, Khojasteh H, Keihan AH, Adib K, Sobhani-Nasab A, Rahimi-Nasrabadi M. Co-precipitation synthesis of Ag-doped $NiCr_2O_4$ nanoparticles: investigation of structural, optical, magnetic, and photocatalytic properties. J Mater Sci: Mater Electron. 2021;32(2):1413–1426. doi: 10.1007/s10854-020-04913-3.
50. Enhessari M, Salehabadi A, Khanahmadzadeh A, Arkat K, Nouri J. Modified sol-gel processing of $NiCr_2O_4$ nanoparticles; Structural analysis and optical band gap. HTMP. 2017;36(2):121–125. doi: 10.1515/htmp-2015-0223.
51. Rasool RZ, Nadeem K, Kamran M, Zeb F, Ahmad N, Mumtaz M. Comparison of anomalous magnetic properties of non-collinear $CoCr_2O_4$ and $NiCr_2O_4$ nanoparticles. J Magn Magn Mater. 2020;514:167225. doi: 10.1016/j.jmmm.2020.167225.
52. Palanisamy G, Kouthaman M, Kandasamy B, Periyasami G, Thangavelu P, Lee J. Rational design of Zn_4O $(BDC)_3$ metal organic framework incorporated with $NiCr_2O_4$ nanoparticles: An affordable photocatalyst for the degradation of hazardous dyes. J Alloys Compd.

2024;1008:176475. doi: 10.1016/j.jallcom.2024.176475
53. Vinothkumar V, Sekhar YC, Chen S-M, Prasad GV, Kim TH. Fabrication of spinel MCr_2O_4 (M= Ni and Co) nanostructures as positive electrode materials for high-performance supercapacitors. J Energy Storage. 2024;92:112185. doi: :10.1016/j.est.2024.112185
54. B. de Castilho et al. Short-time exposure oxidation studies on multi-component coatings and their influence on tribological behavior. Wear, 2021;477(7):203892. doi: 10.1016/j.wear.2021.203892.
55. Lin L, Starostin SA, Li S, Hessel V. Synthesis of metallic nanoparticles by microplasma. Phys Sci Rev. 2018;3(10):20170121. doi: 10.1515/psr-2017-0121.
56. Tan HT, Sun W, Wang L, Yan Q. 2D transition metal oxides/hydroxides for energy-storage applications. ChemNanoMat, 2016;2(7):562–577. doi: **10.1002/cnma.201500177**.
57. Nandagudi A, Nagarajarao SH, Santosh MS, M BB. Hydrothermal synthesis of transition metal oxides, transition metal oxide/carbonaceous material nanocomposites for supercapacitor applications. Mater Today Sustain. 2022;19:100214. doi:
58. Pebley AC. Microplasma jet Synthesis of Ni-Fe oxide films for magnetic exchange bias and electrocatalytic studies. University of California, Santa Barbara, 2017.
59. Geethalakshmi R, Sarada D. Synthesis of plant-mediated silver nanoparticles using Trianthema decandra extract and evaluation of their anti microbial activities. Int J Eng Sci Technol. 2010;2(5):970–975.
60. Kassem MA, El-Fadl AA, Nashaat AM, Nakamura H. Structure, optical and varying magnetic properties of insulating MCr_2O_4 (M= Co, Zn, Mg and Cd) nanospinels. J Alloys Compd. 2019;790:853–862. doi: 10.1016/j.jallcom.2019.03.189.
61. Mohanty P, Prinsloo A, Sheppard C, Roos W. Effect of Fe substitution on structural and magnetic properties of $NiCr_2O_4$. APPA. 2018;133(3):574–577. doi: 10.13140/RG.2.2.17589.17125.
62. Mohamed MA, Jaafar J, Ismail A, Othman M, Rahman M. Fourier transform infrared (FTIR) spectroscopy. in Membrane characterization. In book: Membrane Characterization. Elsevier; 2017. pp. 3–29. doi: 10.1016/B978-0-444-63776-5.00001-2.
63. Ali T, Warsi MF, Zulfiqar S, Sami A. Green nickel/nickel oxide nanoparticles for prospective antibacterial and environmental remediation applications. Ceram Int. 2022;48(6):8331–8340. 2022. doi:
64. Sangwan N, Xia F, Gilbert JA. Recovering complete and draft population genomes from metagenome datasets. Microbiome, 2016;4:8. doi: 10.1186/s40168-016-0154-5.
65. Ramesh C, Kumar KM, Latha N, Ragunathan V. Green synthesis of Cr_2O_3 nanoparticles using Tridax procumbens leaf extract and its antibacterial activity on Escherichia coli. Curr Nanosci. 2012;8(4):603–607. doi: 10.2174/157341312801784366.
66. Abid M, Schilling J, Scheffran J, Zulfiqar F. Climate change vulnerability, adaptation and risk perceptions at farm level in Punjab, Pakistan. Sci Total Environ. 2016;547:447–460. doi: 0.1016/j.scitotenv.2015.11.125.
67. Ezhilarasi AA, Vijaya JJ, Kaviyarasu K, Kennedy LJ, Ramalingam RJ, Al-Lohedan HA. Green synthesis of NiO nanoparticles using Aegle marmelos leaf extract for the evaluation of in-vitro cytotoxicity, antibacterial and photocatalytic properties. J Photochem Photobiol B. 2018;180:39–50. doi: 10.1016/j.jphotobiol.2018.01.023.

